POLAR COLOR MOSAIC PRODUCTION FROM KAGUYA MI DATA. H. Sato[1], S. Goossens[2], M. Ohtake[3], Y. Daket[3], [1]Japan Aerospace Exploration Agency, 3-1-1 Yoshinodai, Chuo-ku, Sagamihara, Kanagawa, Japan (sato.hiroyuki@jaxa.jp), [2]CRESST, University of Maryland, Baltimore County, Baltimore, MD, USA, [3]ARC-Space, the University of Aizu, Japan.

Introduction: During up to 10 months of the actual observation period, SELENE (Kaguya) Multi-band Imager (MI) has achieved over 3400 orbital observations covering ~95% of the lunar surface. Due to the spacecraft's operation in polar orbit, the observation density of the MI increases toward the pole with significant numbers of repeated observations. The mosaic products from multiple observations (for each pixel) can achieve a higher signal-to-noise ratio (S/N) and reduced color artifacts than the single observation. The preliminary product of MI north-polar mosaic from the repeated observations by [1] includes systematic artifacts due to the low accuracy of the spacecraft's position information. Recently [2] improved the Kaguya's SPK, allowing the more accurate coordinates of all the Kaguya observations. Minimizing the geographically mismatched images improves the S/N and photometric normalization by accurate calculations of incidence (*i*), emission (*e*), and phase (*g*) angles. Here we derived a new MI polar color mosaic using the new SPK and evaluated the accuracy of derived reflectance.

Methodology: We used the MI images (9 bands from 415 to 1550 nm; ~20 m/pixel in visible, ~62 m/pixel in NIR)[3] with the center latitude of each image above 80°S (16,762 images, Fig. 1), acquired from November 2007 to Jun 2009. The DN values of all images were radiometrically calibrated to the radiance factor (***I/F***) [4]. The pixel coordinates were derived by the SPICE toolkit [5] with the new SPK [2].

The ***i*** and ***e*** angles were computed based on the local topography from Lunar Orbiter Laser Altimeter (LOLA) gridded data records (20 m/pixel) [6]. From the coordinate of each pixel and the locations of the spacecraft and the Sun at the time of each observation, we computed the ***i***, ***e***, and ***g*** angles.

Next, we calculated the photometric parameters using Hapke model [4]. Instead of deriving the Hapke parameter maps [7], we derived a single set of parameters to obtain enough angle variations of ***i*** and ***e***. Then we derived the photometrically normalized ***I/F*** (***nI/F***) by the single parameter set. Since the south polar region is dominantly the highlands, we assumed that our studied area is photometrically uniform. For the parameter calculation sampling site, we selected a rectangular region (Fig. 1 red box) where there are no extensive immature ejecta deposits.

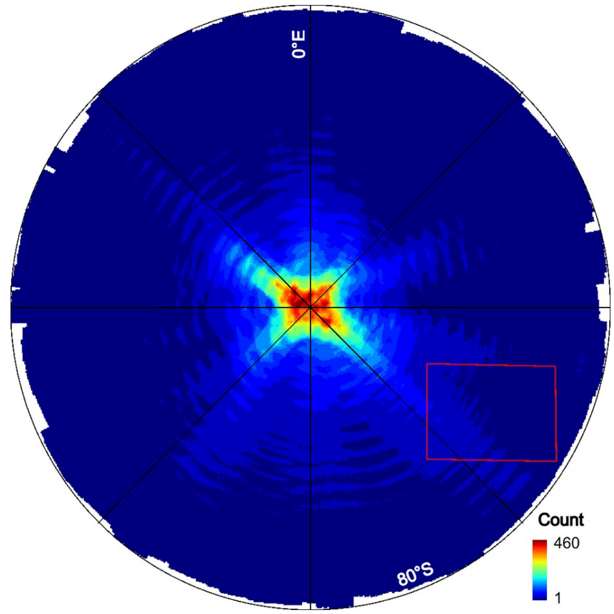

Figure 1. Number of repeated observations by the MI above 80°S in ~1 km/pixel. Black lines indicate latitude 80°S; longitude from 0°E to 270°E (clockwise). Red box outlines the sampling site for the Hapke parameter calculation.

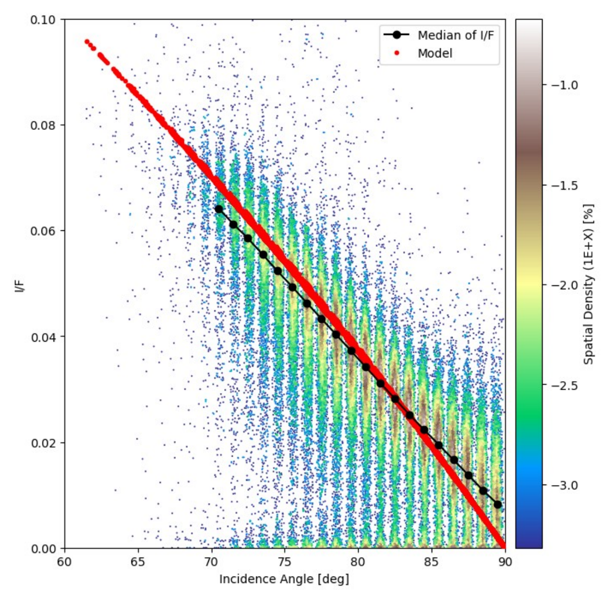

Figure 2. Density plot of the incidence angle (***i***) vs ***I/F*** in 1550 nm band. Red and black lines correspond to the model fit and the median of ***I/F*** in each 1° bin, respectively. The vertical stripes are caused by down-sampling (binning of ***i***, ***e***, and ***g*** angles in 1° for each MI image before accumulating all the data inside the sampling site).

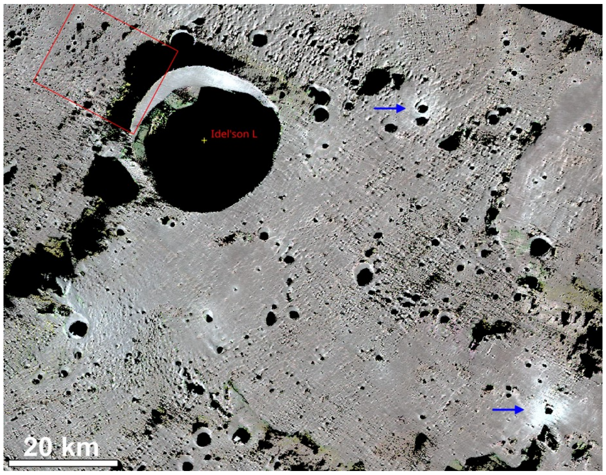

Figure 3. RGB color composite (R:1550 nm, G:1000 nm, and B: 900 nm) of MI median mosaic. Red box indicates the area shown in Fig. 4. The area of this figure is indicated by Fig. 1 red box. Blue arrow indicates the fresh crater ejecta.

From all the overlapping observations, we computed a median of ***nI/F*** for each pixel value of the final mosaic product (hereafter called "median mosaic").

Results: The number of repeated observations within the south-pole region (>80°S) ranged up to 460 and 26.3 on average (Fig. 1). The pole has the highest density due to Kaguya's polar orbit operation.

The curve-fit on the observed ***I/F*** for the Hapke parameter calculation (Fig. 2) achieved a fitting error of about 0.4% in the averaged value. The offset relative to the median of each bin (Fig. 2 black line) is caused by local undulations unresolved by the topography data, which add the scatters and increase the averaged level of ***I/F*** at ***i*** close to 90°.

The RGB composite map of the MI median mosaic (Fig. 3) exhibits flat with no topographic relief (except the sharp shadows) nor color artifacts, indicating that the photometric normalization was performed with enough accuracy. The high reflectance of immature ejecta of the small craters (~1.5 km in diameter, Fig. 3 blue arrows) are clearly displayed, demonstrating the potential for the albedo studies in the polar regions. The parallel wrinkles extending from lower-left to upper-right in the image (perpendicular direction to the pole) are possibly the small topographic undulations that frequently cause sub-pixel shadows.

Discussion: The sharp topographic boundaries in the median mosaic (Fig. 3) indicates that the new SPK has enough accuracy to match the features pixel-by-pixel in multiple images acquired in different orbits.

The shadows cast from the topographic summits and ridges (e.g., crater rim) often result in inaccurate ***nI/F***. The southern rim of Idel'son L crater, for

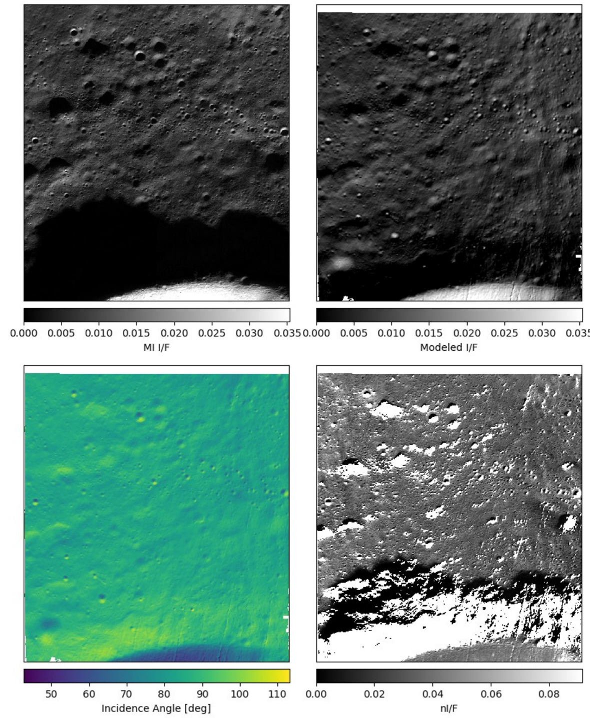

Figure 4. Sample MI image (ID: 03_04747S848E1173) in ***I/F*** (upper left), modeled ***I/F*** derived by Hapke model (upper right), incidence angle layer (lower left), and ***nI/F*** (lower right). Southern rim of Idel'son L crater is shown in the bottom of all images. In the bottom right panel, the dark zone above the shadowed region (white null pixels) corresponds to abnormal ***nI/F*** area, caused by the unpredicted shadow.

example, makes a long shadow (~7.2 km, Fig. 4 top left). These shadows are not predictable from the incidence angles. Thus the modeled ***I/F*** (Fig. 4 upper right) is unable to recreate accurate shadow areas, resulting in the low ***nI/F*** zone along the crater rim. It is hard to detect such shadowed areas by setting thresholds on ***nI/F*** because the shadows are vaguely-outlined by indirect lighting from the nearby slopes. The effect of the Sun disk fraction, which is emphasized in long shadows, also causes faint shadows. An illumination simulation by ray-tracing can predict the exact area of faint shadows that allows improving the accuracy of ***nI/F*** and the mosaic colors.

References: [1] Sato et al. (2018) *New Views of the Moon 2 – Asia*, abstract #6011. [2] Goossens et al. (2020) *Icarus* 336, 113454. [3] Kodama, S. et al. (2010) *Space Sci. Rev.*, v154, 1-4, p79-102. [4] Hapke, B. (2012) *Cambridge Univ. Press*, NY. [5] Acton, C. H. et al. (1996) *Planet. Space Sci.*, v44, p65-70. [6] Smith et al. (2010) *GRL*, 37(18). [7] Sato et al. (2014) *JGR-Planets*, 119(8), 1775–1805.